



# Three-dimensional modeling of frontal polymerization for rapid, efficient, and uniform thermoset composites manufacturing

Amirreza Tarafdar<sup>a</sup>, Chen Jia<sup>b</sup>, Weifei Hu<sup>b</sup>, Ian D. Hosein<sup>c</sup>, Kun (Kelvin) Fu<sup>d</sup>, Yeqing Wang<sup>a,\*</sup>

<sup>a</sup> Department of Mechanical and Aerospace Engineering, Syracuse University, Syracuse, NY, 13244, USA

<sup>b</sup> School of Mechanical Engineering, Zhejiang University, Hangzhou, 310058, China

<sup>c</sup> Department of Biomedical and Chemical Engineering, Syracuse University, Syracuse, NY, 13244, USA

<sup>d</sup> Department of Mechanical Engineering, University of Delaware, Newark, DE, 19716, USA

## ARTICLE INFO

Handling Editor: Dr Hao Wang

### Keywords:

Frontal polymerization  
Finite element analysis  
Cross-ply laminate  
Triggering direction  
Efficient manufacturing

## ABSTRACT

Due to the incapability of one-dimensional (1D) and two-dimensional (2D) models in simulating the frontal polymerization (FP) process in laminated composites with multiple fiber angles (e.g., cross-ply, angle-ply), modeling a three-dimensional (3D) domain, which is more representative of practical applications, provides critical guidance in the control and optimization of the FP process. In this paper, subroutines are developed to achieve the 3D modeling of FP in unidirectional and cross-ply carbon fiber laminates with finite element analysis, which are validated against the experimental data. The 3D model is employed to study the effect of triggering direction in relevance to the fiber direction on the FP process, which cannot be studied using traditional 1D/2D models. Our findings suggest that triggering in the fiber direction leads to a higher front velocity, in comparison to cases where front was triggered in the direction perpendicular to the fiber. Moreover, the average front velocity in cross-ply laminates is on average 20–25% lower than that in unidirectional laminates. When triggered using two opposite fronts in the in-plane direction, the maximum temperature of the thermal spike in the cross-ply laminate, when two fronts merge, is about 100 °C lower than that in the unidirectional laminate. In cross-ply laminates, a sloped pattern forms across the thickness direction as the front propagates in the in-plane direction, as opposed to the traditionally observed uniform propagation pattern in unidirectional cases. Furthermore, the effect of thermal conductivity is studied using two additional composite laminates with glass (1.14 W/m-K) and Kevlar fibers (0.04 W/m-K). It is shown that the frontal velocity, degree of cure, and the thermal spike temperature decrease as the thermal conductivity reduces.

## 1. Introduction

The manufacturing methods of thermoset-based fiber reinforced composites considering the cost, the ease, and the time-consuming issues, have a significant impact on industries and economy, due to their extensive potential to be employed in different structural applications. The manufacturing process for thermoset-based composites relies on the polymerization process, which typically leads to a prolonged heating cycle, significant energy consumption, and environmental damage, with the costs escalating exponentially with the size of the structure [1–5]. Frontal polymerization (FP), an emergent alternative among various manufacturing methods (e.g., reactive extrusion [6,7], microwave curing [8], ultraviolet (UV) photocuring [9–11], vacuum assisted resin transfer molding (VARTM) [12,13], thermal press curing [14], hand

laying-up [15]), employs a self-propagating exothermic reaction zone, named “the curing front”, which converts a monomer into a polymer, providing a rapid and more energy-efficient method of manufacturing thermoset-based composite structures [16,17]. This manufacturing method features a self-sustained process, since the generated heat propagates forward and drives the curing front through the entire monomer [16,18]. Several polymeric materials, including thermoset monomers, functionally graded polymers, hydrogels, nanocomposites have been synthesized using FP [19–28]. Among these materials, the FP of dicyclopentadiene (DCPD) resin presents high energy density, high reactivity, and low viscosity [29,30]. Moreover, due to its high fracture toughness, impact resistance, stiffness, and chemical resistance [29], the DCPD is a thermoset polymer appropriate for the manufacturing of durable resin and fiber reinforced plastic composites. As a result, the

\* Corresponding author.

E-mail address: [ywang261@syr.edu](mailto:ywang261@syr.edu) (Y. Wang).

<https://doi.org/10.1016/j.compositesb.2023.111029>

Received 27 June 2023; Received in revised form 12 September 2023; Accepted 26 September 2023

Available online 5 October 2023

1359-8368/© 2023 Elsevier Ltd. All rights reserved.

fabrication of composites with DCPD resin would be a point of interest to benefit from its appropriate material properties.

The demand for carbon fiber reinforced polymer (CFRP) matrix composites is nowadays integral to aerospace, civil infrastructure, marine, automotive, and the transportation sector, due to the light weighting and extraordinary mechanical properties, including high specific strength and stiffness, excellent energy absorbing properties. The main factors for manufacturing these composites using the FP method are the rate of the polymerization and cure front velocity, which have an impact on the amount of the matrix penetration into the carbon fiber and mechanical properties of the final product [31–34]. Due to its high rate of the polymerization, the FP is particularly intriguing and has the potential to enable rapid production of massive structural components [35]. Thus, fabricating CFRP consisting of a compatible thermoset-based resin, such as DCPD and epoxy resin, via the FP method is a promising technique to achieve proper material properties alongside with reducing overall costs associated to the manufacturing process. Tran et al. [36] successfully cured the thermoset-based composites which contains up to 40 vol% of short fiber employing the radical induced FP. They investigated the effect of different fiber volume fraction and weight contents of the thermal initiator. It was revealed that CFRP laminate with 40 vol% fiber and 10% thermal initiator exhibited high storage stability. In a research by Robertson et al. [16], it was reported that the mechanical properties, including the tensile strength, Young's modulus, and the fracture toughness of neat DCPD and CFRP with DCPD matrix are comparable to those fabricated through the conventional oven curing method.

To guide the control and optimization of the FP process, predictive modeling studies have recently been reported. For example, Solovyov et al. [37] proposed a model which predicts the propagation of the cure front in a highly exothermic reaction for FP of methacrylic acid and n-butyl acrylate monomers. In another study, Goldfeder et al. [38] developed a mathematical model based on the structure of polymerization wave, front velocity, temperature, and degree of conversion of monomer. These two models investigate the FP process in pure resin by coupling the degree of conversion with the heat diffusion formulation. Studies have identified several key factors in the FP of composites, including the cure kinetics, operating temperature, and thermal conduction [39–41]. In light of this, finite element models can be greatly simplified by using phenomenological models based on a cure kinetics relation rather than solving for the monomer's conversion. For example, Goli et al. [35] employed a one-dimensional (1D) finite element approach to solve the transient, coupled diffusion-reaction equations to characterize FP in unidirectional carbon fiber composites with DCPD resin. They examined the front velocity, as well as the thermal and degree of cure characteristics in the local region of the front, using a homogenized fiber and matrix composite model. Triggering of FP along the fiber direction, they also showed that front velocity increased by increasing the fiber volume fraction from 0 to 15% but decreased with higher fiber volume fractions. The competing mechanisms between the exothermic heat generation and the heat diffusion in the carbon fiber tows are perceived to have caused this behavior.

In addition to the heat diffusion through the resin, the thermal properties of fiber significantly affect the propagating mechanisms of the curing front [42,43]. Carbon fibers accelerate the front velocity at low fiber volume fractions, due to the high thermal conductivity. Recently, Wang [44] employed a two-dimensional (2D) reaction-diffusion model to predict the effect of the microstructure characteristics on the FP behavior of unidirectional CFRP. In contrast with the previous studies, the fiber and the matrix are modeled as two separate domains for better comprehension of effects of the fiber volume fraction, fiber tow size, and fiber tow shapes. The results showed that the fiber volume fraction and the tow shape (e.g., circular or elliptical cross section) have major impact on the characteristics of FP in contrast with the fiber tow size.

Although recent modeling attempts have been made for FP of CFRP

composites [17,18,35,40,43,45], these models have focused on 1D and 2D configurations, which are insufficient to study FP in laminated composites with multiple fiber angles, such as cross-ply and angle-ply laminates. These composites are widely known to be more representative of those used in the industry. Without 3D models, one cannot investigate how the composite layup and other factors affect the FP process of composites with multiple fiber angles. Extending the current 1D and 2D models into 3D is challenging, due to the numerical treatment of coupling the heat transfer and cure kinetics equations in a 3D computational domain. In this paper, user subroutines are developed including, HETVAL (i.e., heat flux subroutine) and USDFLD (i.e., user defined field subroutine) to accommodate the numerical treatment using the finite element software ABAQUS, which are validated against experimental data. This proposed 3D model models the fiber tow and the DCPD as separate geometric domains, which are different from the existing 1D and 2D models, which homogenizes the fiber tow and the DCPD resin as a smeared part. By modeling the fiber tow and DCPD resin separately allows us to uniquely capture the effects of layup and triggering directions on the FP process, which cannot be achieved in existing 1D and 2D models. The 3D model is also employed to study the effect of thermal conductivity of the fiber on the FP process of the composite laminates.

## 2. Problem description

### 2.1. Thermo-chemical formulation of neat DCPD resin

The thermo-chemical relation between the heat transfer problem and the front propagation in a neat DCPD resin is mathematically governed by a classical heat condition equation for the temperature  $T$  and the degree of cure  $\alpha$ . The heat is generated by an enthalpic reaction, which is formulated as:

$$k \left( \frac{\partial^2 T}{\partial x^2} + \frac{\partial^2 T}{\partial y^2} + \frac{\partial^2 T}{\partial z^2} \right) + \rho H_r \frac{\partial \alpha}{\partial t} = \rho C_p \frac{\partial T}{\partial t} \quad (1)$$

where  $k$  represents the thermal conductivity,  $\rho$  is the density,  $C_p$  indicates the specific heat,  $H_r$  is defined as the total enthalpy of reaction (for the resin only). This mathematical model is solved for fiber tow and matrix separately in the 3D domain using their corresponding material properties. To define the relation between temperature ( $T$ ) and degree of cure ( $\alpha$ ), the Arrhenius equation with the classical Prout-Tompkins (PT) autocatalytic model is utilized:

$$\frac{\partial \alpha}{\partial t} = A \exp \left( -\frac{E}{RT} \right) (1 - \alpha)^n \alpha^m \frac{1}{1 + \exp [C(\alpha - \alpha_c)]} \quad (2)$$

where  $A$ ,  $E$ ,  $n$ ,  $m$ ,  $C$ , and  $\alpha_c$  are cure kinetics characteristics. These parameters can be obtained by conducting Differential Scanning Calorimetry (DSC) experiments and fitting the rate of cure curve. The corresponding values of the cure kinetics parameters and the material properties of the DCPD resin are presented in Table 1 [16].

### 2.2. Problem setup

In this study, the effect of triggering direction, including directions that are parallel and perpendicular to the fiber direction are studied in unidirectional and cross-ply CFRP composite laminates. Moreover, laminates with glass and Kevlar fibers are considered to investigate the effect of thermal conductivity on the temperature profile and evolution of the degree of cure in comparison with laminates with carbon fiber. Throughout our study, the unidirectional composite laminate is specified by a letter "U" and the cross-ply laminate is denoted by "C". Letters followed by that in the label represent the triggering direction. For example, the label "UT" represents the unidirectional case where the front is initiated from the top side (see Fig. 1) through the thickness direction. For both unidirectional and cross-ply laminates, "L"

**Table 1**  
Material properties and curing kinetics parameters of the DCPD [16,44].

Material properties				Curing kinetics characteristics			
Density ( $\rho$ )	Thermal conductivity (k)	Specific heat ( $C_p$ )	Total enthalpy of reaction ( $H_r$ )	Pre-exponential coefficient (A)	Activation energy (E)	Orders of reaction	Diffusion parameters
980 (kg/m <sup>3</sup> )	0.15 (W/m·K)	1600 (J/kg·K)	350 (J/g)	8.55e15 (s <sup>-1</sup> )	116.75 (kJ/mol)	$n = 1.72$ $m = 0.77$	$C = 14.48$ $\alpha_c = 0.41$

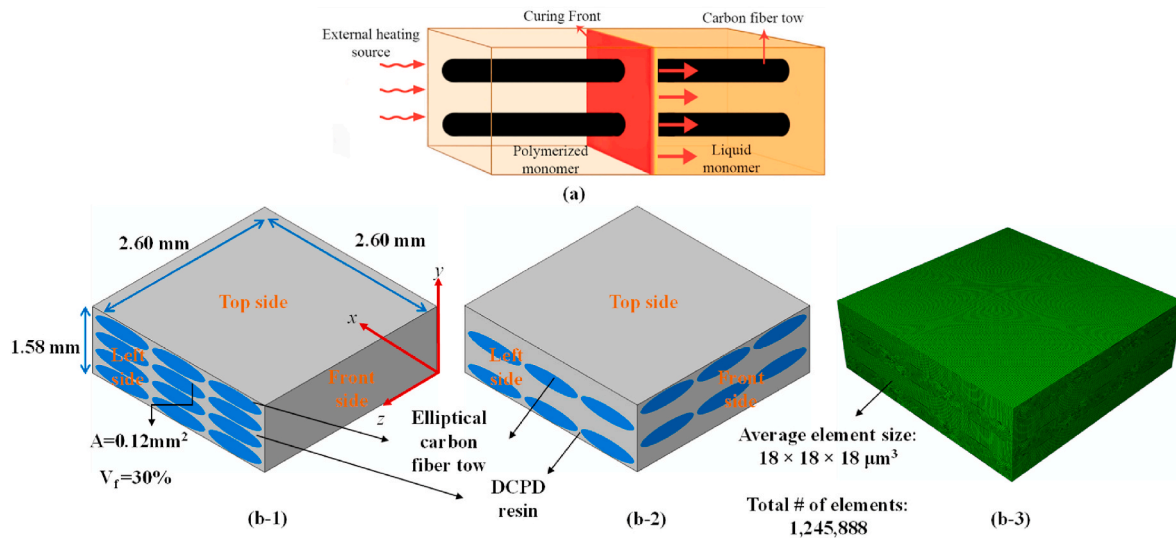


**Fig. 1.** Problem configuration of the FP of CFRP/DCPD resin composites: (a) schematic representation of frontal polymerization process, geometric representation of (b-1) unidirectional, (b-2) cross-ply laminate, and (b-3) the meshed model of the cross-ply laminate.

represents cases where the front is initiated from the left side, “LR” represents cases where two fronts are initiated from both the left and right sides, “F” represents cases where the front is triggered from the front side, and “FB” represents cases where the front is triggered from both the front and back sides. These sides for the unidirectional and cross-ply laminates are depicted in Fig. 1.

Fig. 1 shows a schematic of frontal polymerization process and the geometrical representation of unidirectional and cross-ply CFRP composites. The computational size is consistent with the 2D model in our prior work [44], where the effect of the computational size on the FP process was reported and not repeated here for brevity. The fiber volume fraction is 36%, which is also consistent with prior work [44]. The other reason for such a choice is that increasing the fiber volume fraction decreases the degree of cure, front velocity, and front temperature [16, 41, 46]. The fiber volume fraction of 36% is conservative and has been achieved in the experiments [18]. For the elliptical cross section of the fiber tow, the cross-sectional area is 0.12 mm<sup>2</sup>, which represents a 3 K tow of HexTow AS4 carbon fiber [47]. Note that the fiber tows are twisted during the weaving process which results in an elliptical cross section of the fiber [48–51]. Moreover, the ratio between the larger radius and the smaller radius of the elliptical cross section is set to 4. Our prior work [44] reported that the fiber volume fraction and fiber tow shape have a significant effect on the maximum temperature and the front velocity during the polymerization. Also, increasing the ratio between the larger and the smaller radii of the ellipse caused the maximum temperature and the front velocity to decrease. Furthermore, due to the high thermal conductivity of the carbon fiber (*i.e.*, 10.45 W/m·K [16]), increasing the fiber volume fraction causes more volumetric heat to be consumed, which is generated in the FP process, thereby decreasing the heat required for propagating the front and reducing the front temperature and finally the degree of cure. Moreover, it was reported that the void volume for DCPD resins fabricated using FP is about 0.15% [16, 44, 46]. Therefore, the effect of the void contents is considered negligible

and not considered in our simulations.

Note that to capture the resin infiltration within the fiber tow, we homogenized the individual fiber filaments in the fiber tow and the resin, but only in terms of the thermal properties (*i.e.*, thermal conductivity, specific heat). The geometric domain of the fiber tow is kept as an integral solid part because the majority volume of the fiber tow is taken by the solid fiber filaments, where the resin only flows through the voids within the fiber tow. If we homogenize the fiber tows, it will permit the front to propagate through the entire domain of the fiber tow, which does not represent the true condition, where the resin only flows through the voids within the fiber tow. To provide a more accurate and detailed prediction of the FP within the fiber tow, a microscopic intra-tow model will need to be developed and integrated into the current 3D model, which will be a subject of our future work.

### 2.3. Numerical simulation

The built-in heat transfer step of ABAQUS only enables the user to simulate the general heat transfer problem. However, the heat generated during the polymerization process is an internal heat caused by the enthalpic reaction, which cannot be directly simulated using the ABAQUS built-in heat transfer step. To solve this problem, we developed a heat flux subroutine (*i.e.*, HETVAL) and a user defined field subroutine (*i.e.*, USDFLD). These subroutines are used together to solve the heat transfer equations by incorporating the rate of cure ( $\partial\alpha/\partial t$ ) at each integration point and each time increment. Specifically, the rate of cure is stored as a solution-dependent state variable (*i.e.*, SDV1) in the USDFLD subroutine. The accumulation of the product between the rate of cure and the step time will allow us to calculate the degree of cure ( $\alpha$ ), which is stored as another solution-dependent state variable (*i.e.*, SDV2). Then, the rate of cure will be passed to the HETVAL subroutine to update the volumetric heat flux in the heat transfer equation, which is solved to obtain the temperature for the next time increment. It was employed

here for a 3D model to investigate three design parameters which are mentioned in the previous section in both cross-ply and unidirectional CFRP composites with DCPD resin. The density, thermal conductivity, and the specific heat of the carbon fiber, glass fiber, and Kevlar fiber are listed in Table 2. Note that the material properties of the DCPD resin are shown in Table 1.

The initial and boundary conditions are as follows:

$$T|_{t=0} = T_0 = 23\text{ }^\circ\text{C} \text{ and } \alpha|_{t=0} = \alpha_0 = 0.07 \quad (3)$$

$$T_{\text{trig}} = 220\text{ }^\circ\text{C}, 0 \leq t \leq t_{\text{trig}}, \text{ applied at different triggering sides} \quad (4)$$

where Eqs. (3) and (4) denote the initial condition, including the initial temperature ( $T_0$ ) and the initial degree of cure ( $\alpha_0$ ). Note that the value of  $\alpha_0$  is obtained from the experimental study [16]. The triggering time duration,  $t_{\text{trig}}$ , and triggering temperature,  $T_{\text{trig}}$ , are chosen as 3.5 s and 220 °C, respectively in accordance with the reported experiments [16, 44]. It should be noted that unspecified thermal boundary conditions are set as insulated boundary conditions. Moreover, based on our preliminary studies and the results in Ref. [53], the convection and radiation BCs play insignificant roles in the heat transfer and FP process due to the short duration of the process, which are therefore not considered in the simulation.

The 8-node linear heat transfer quadrilateral brick elements are used to mesh the 3D domain (*i.e.*, DC3D8 in ABAQUS). The model is meshed by an extremely fine mesh with an average element size of  $18 \times 18 \times 18 \mu\text{m}^3$  (see Figs. 1(b-3)). Prior mesh dependency research has confirmed that mesh-independent results can be attained using current mesh settings.

### 3. Model validation

The proposed subroutines for the finite element analysis model is validated against the experimental data in Ref. [16]. In the experiments, the DCPD resin is placed within a glass test tube with a 5.50 mm radius and a 1 mm wall thickness. A single carbon fiber tow consisting of 3 k individual carbon fiber filaments is located at the center of the glass tube. The polymerization is initiated using a soldering iron on the opening side of the glass tube. Noted that the external heat source was applied only to the monomer to ensure that the heat is diffused via the monomer rather than the fiber tow. Additionally, a two-dimensional axisymmetric model was generated to reduce the computational cost, due to symmetry of the problem along the center axis of the glass tube. The problem configuration is illustrated in Fig. 2(a). By comparing the experimental findings in Ref. [16] and simulation results, the 2D model followed the same propagation pattern when compared to optical measurements (Fig. 2(b)). The average front velocity resulted from the simulation (1.07 mm/s) shows good agreement with experimental data. The maximum temperature of numerical results is 223 °C (Fig. 2(c)), which also agrees well with the maximum temperature in the experiment (220 °C).

To further validate the 3D model, additional validation cases are performed for a unidirectional carbon fiber composite laminate with varying fiber volume fractions (*i.e.*, 0–50%). The frontal velocity and the maximum temperature vs. fiber volume fraction predicted by the 3D modeling are compared with those by 1D and 2D modeling and the experimental data [18]. The detailed description and results are

**Table 2**  
Thermophysical properties of carbon fiber, glass fiber, and Kevlar fiber [41,44, 52].

	Density (kg/m <sup>3</sup> )	Thermal conductivity (W/m-K)	Specific heat (J/kg-K)
Carbon	1760	10.45	795
Glass	2230	1.14	800
Kevlar	1440	0.04	1420

included in the supplementary file. It is shown that the 3D modeling exhibits a high level of concordance with the 1D and 2D modeling and the experimental data.

## 4. Results and discussions

### 4.1. Effect of laminate layup and triggering direction

Simulation videos for all studied cases showing the evolution of the degree of cure field in the unidirectional and cross-ply laminates are extracted and can be found in the supplementary file.

Table 3 shows the effect of the triggering direction on the FP characteristics, including the initial curing duration, average front velocity, and average degree of cure, for unidirectional composite cases. Note that the initial curing duration is chosen as the duration when the curing front initially reaches the opposite surface of the triggering surface. The average front velocity is calculated by dividing the actual distance that the front propagated over the corresponding duration. The results showed that the front triggering direction significantly affects the front velocity and the curing time. Generally, the curing duration is longer than 0.40 s for the considered unidirectional cases, except for the case with multiple triggering direction (*i.e.*, ULR), which shows a much faster polymerization with a curing duration of only 0.14 s. Moreover, the UF specimen is much less cured (24.80% degree of cure) at the end of the analysis, where the average front velocity and degree of cure are lowest among all unidirectional cases.

Fig. 3 illustrate the FP history of the UT case, where the front is triggered from the top surface, including the degree of the cure contours and temperature history. Fig. 3(a) shows the temperature profiles extracted along the y direction at varying times (*i.e.*, along the path highlighted in red in the inset of Fig. 3(a)). Fig. 3(b) and (c) show the evolutions of the degree of cure captured in front and left side views, respectively. As we can see, as the front initiates from the top surface, the higher thermal conductivity of carbon fibers than the DCPD resin, along with the uniform distribution of carbon fiber tows, causes the front to propagate quickly to the bottom surface. On the other hand, due to the thermal insulating boundary condition, the heat generated in each stage is trapped in the specimen, which results in increasing the temperature up to 220 °C (see Fig. 3(a)). Moreover, due to the bottom surface being insulated, at  $t = 1.10$  s, the curing front travels backward to the top surface, resulting in the further polymerization of the UT specimen. When comparing the temperature history and the degree of cure at 0.50 s and 1.10 s, it can be observed that the maximum temperature dropped from 300 °C to 180 °C (Fig. 3(a)). During the upward movement of the curing front, the middle part of the laminate is cured up to 94.30% (see Fig. 2(b-3) and (c-3)). At the end of the step at  $t = 3.50$  s, only regions near the top and bottom surfaces have achieved a cure of above 95%, due to the top and bottom surfaces being thermally insulated.

The degree of cure contours and temperature profiles at varying times for UL and ULR cases are illustrated in Figs. 4 and 5. In Fig. 4 (b) and 4(c), the cure front exhibits a symmetric shape as the front is initiated from the left side of the specimen. The elliptical cross section of the fiber tow influences the heat transfer in the surrounding DCPD resin. Specifically, since carbon fiber has a higher thermal conductivity than the DCPD resin, the front in regions between adjacent carbon fiber tows propagates further into the fiber direction, as indicated in the Fig. 4(b-1) and 4 (c-1). As the temperature rises to 260 °C, in regions near the triggering side (Fig. 4(a)), the front velocity in regions between two adjacent carbon fiber tows is accelerated. In other words, the heat transfer and the increasing temperature in the DCPD resin cause the front in regions between adjacent carbon fiber tows to propagate with a higher velocity than in other regions, as shown in Fig. 4(b-1) and 4 (c-1). This pattern is observed in the FP process until the curing front first arrives the opposite side of the laminate. After that, the curing front travels backward towards the triggering side of the domain. This phenomenon has also been observed in the UT specimen (Figs. 3(c-2)).

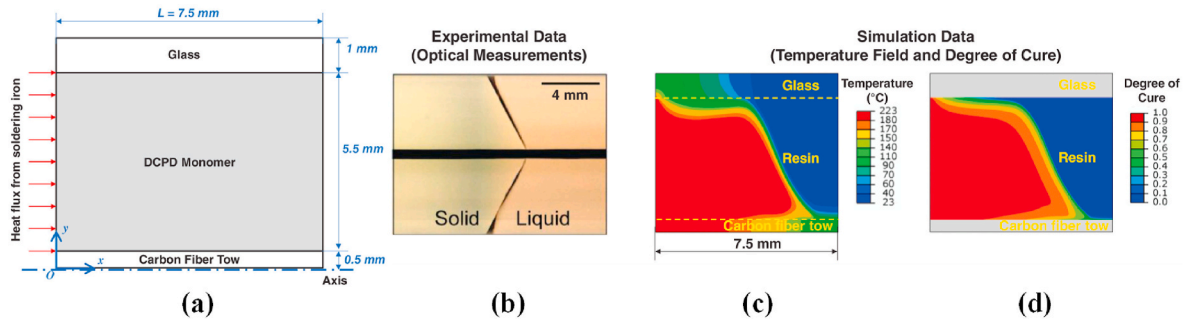


Fig. 2. Illustrations of (a) problem configuration for model validation, (b) experimental optical measurement, (c) evolution of temperature field and (d) degree of cure for DCPD resin with a single carbon fiber tow at the center of the glass tube.

Table 3

Comparison of frontal polymerization (FP) process characteristics of unidirectional laminates with different triggering directions.

Specimen	Initial curing duration (s)	Average front velocity (mm/s)	Average degree of cure (%)
UT	0.48	1.80	94.30
UL	0.42	6.17	95.30
ULR	0.14	9.13	99.50
UF	Not fully cured	0.27	24.80
UFB	1.11	1.16	77.30

However, the curing time for the UL specimen is much lower than that of the UT specimen, indicating a much faster polymerization.

It should be mentioned that the predicted front velocity of  $6.17\text{ mm/s}$  for the UL case is two times faster than the front velocity reported in Ref. [18]. The reason for this difference is that the geometry and boundary conditions used in the experiment [18] are completely

different from those used in our simulations. First, the size of our computational domain (*i.e.*,  $2.60\text{ mm} \times 2.60\text{ mm} \times 1.58\text{ mm}$ ) is much smaller than that of specimens used in the experimental tests (*i.e.*,  $10\text{ cm} \times 20\text{ cm}$ , thickness not mentioned). As reported in our prior work [44], scaling up the dimension of the model decreases the front velocity. For example, for a computational domain with a thickness of  $3.50\text{ mm}$ , the front velocity is about 60% slower than the case when using an equivalent domain with a thickness of  $2.60\text{ mm}$ . Second, the boundary conditions used in our model are assumed to be an ideal insulation, which is different from the experimental setup, in which the PDMS substrate or polyurethane rubber gasket could still allow the heat exchange with the ambient environment. The difference in the boundary conditions influences the amount of trapped heat within the specimen, which has caused the differences in the front velocity.

By comparing Fig. 3(a) to Fig. 4(a), it can be seen that the temperature increases up to  $320\text{ }^\circ\text{C}$  when the curing front reaches the opposite side of the UL specimen, in comparison with the temperature in the UT

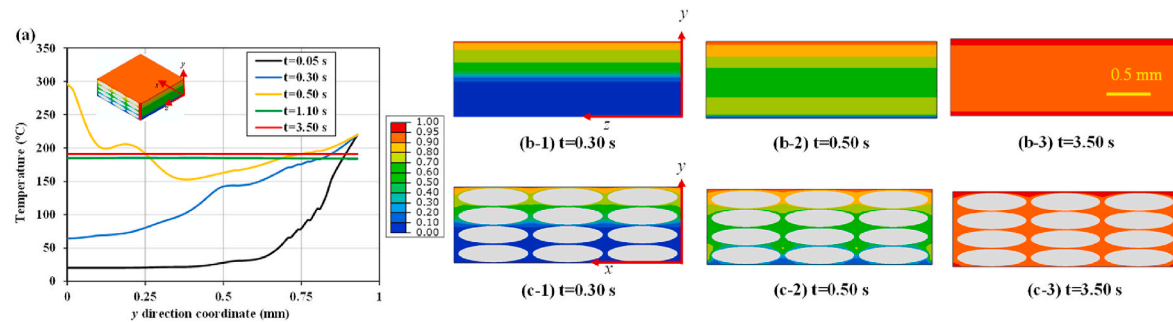


Fig. 3. (a) Temperature profiles along the y direction, (b) and (c) evolution of the degree of cure for UT specimen in the y-z and x-y planes.

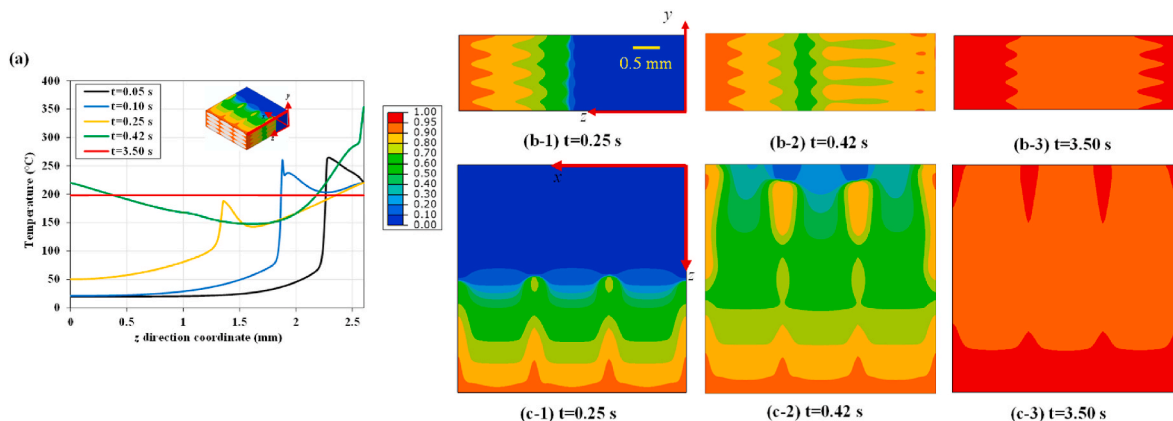


Fig. 4. (a) Temperature profiles along the z direction, (b) and (c) evolution of the degree of cure field for UL specimens in the y-z plane and in the x-z plane.

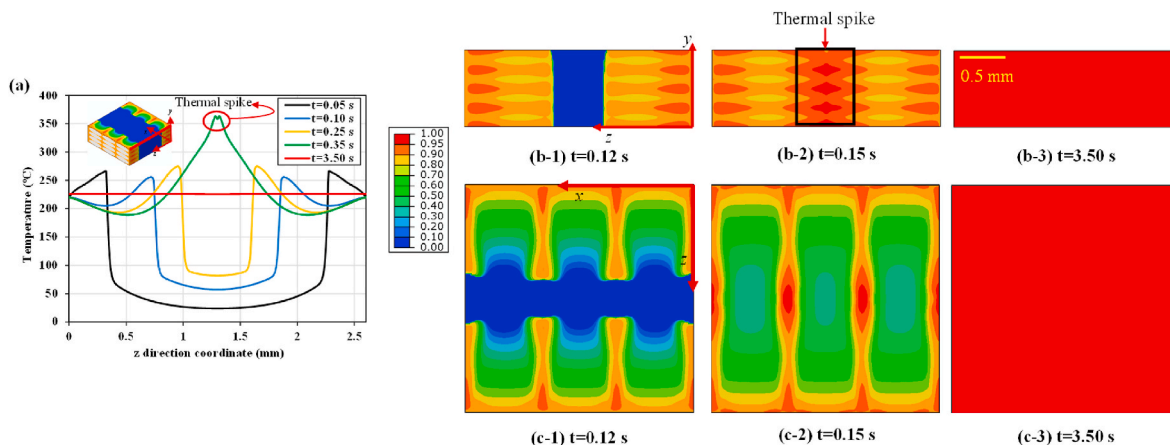


Fig. 5. (a) Temperature profiles along the z direction, (b) and (c) evolution of the degree of cure field for ULR specimens in the y-z plane and in the x-z plane.

specimen, which is 280 °C. This indicates that when the front is triggered in the direction parallel to the fiber tow direction, the FP can be significantly accelerated (about 2.43 times faster), when compared to the case when the front is triggered in the direction perpendicular to the fiber. As shown in Fig. 4(a), the temperatures remain higher than 150 °C through the whole UL specimen, in contrast with the UT specimen (see Fig. 3(a)). It should be noted that the higher temperatures in the UL specimen result in a higher degree of cure in the UL specimen (up to 95.30%), when compared to the that in the UT specimen (up to 94.30% in the middle regions), at the end of the analysis step.

Results in Fig. 5 illustrate the FP process in the ULR case. It can be seen, the initial propagation pattern of the curing front in the ULR specimen is identical to the UL specimen. By comparing Fig. 5(b-1), 5(b-2), 5(c-1), and 5(c-2), the degree of cure achieved 80–95% for ULR with a duration of 0.12 s, whereas the UL case only achieved 60–75% but with a much longer duration of 0.35 s. In addition, as shown in Fig. 5(b-2) and 5(c-2), once the left and right curing fronts collide, a thermal spike forms. This thermal spike phenomenon has also been experimentally observed in a study reported by Centellas et al. [46] for woven CFRP composites. Our predicted temperature escalates dramatically up to 360 °C in the middle part of the specimen. After that, the two fronts travel backwards, which results in an increase in the degree of cure and a steady temperature of 230 °C. This left-right movement of the fronts with a lower velocity causes the ULR specimen to be highly cured at the end of the process (as shown in Fig. 5(b-3) and 5(c-3)). In Fig. 5(a), (b),

and 5(c), it can be seen that our computational domain possesses a sufficiently large interaction distance between two fronts to capture the merging of the thermal spike. Specifically, Fig. 5(b-1) and 5(c-1) show that the two fronts did not interact until they both reach to the middle. Before that, the two fronts propagate independently.

The results for the UF and UFB cases are presented in Figs. 6 and 7. The degree of cure in the UF and UFB specimens is, on average, 20% and 70%, respectively, lower than those in the ULR, UL, and UT cases. According to Figs. 6(b-1), the front is formed at approximately 0.50 s. A portion of the supplied heat is consumed to increase the temperature of the carbon fiber tow, where the rest of the heat is transferred to the lateral side of the carbon fiber tow to the DCPD resin domain to drive the cure front. It can be noticed that the volumetric heat is trapped in regions between two adjacent carbon fiber tows in the initial stages. Subsequently, the temperature lowers down to 80 °C (Fig. 6(a)) and the average degree of cure only reaches to 24.80%. At the end of the step, less than one third of the UF specimen is cured.

For the UFB specimen, the FP process is similar to the UF case. By comparing to the ULR model (see Fig. 5(b) and (c)), the average front velocity in ULR is 7 times higher than that in UFB. Additionally, the degree of cure is about 80% in ULR, in comparison with 65–70% degree of cure in UFB. On the other hand, the thermal spike is not observed in the UFB. The maximum temperature for the UFB specimen is only about 140 °C, whereas the temperature dramatically increased up to 360 °C in the ULR specimen (see Fig. 5(a) at  $t = 0.35$  s).

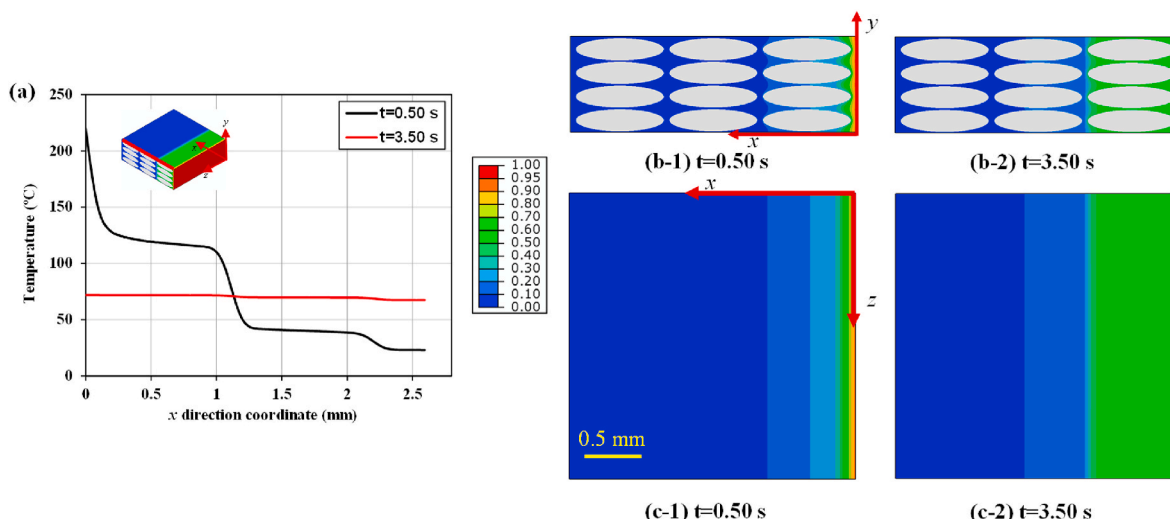


Fig. 6. (a) Temperature profiles along the x direction, (b) and (c) evolution of the degree of cure field for UF specimen in the x-y plane and in the x-z plane.

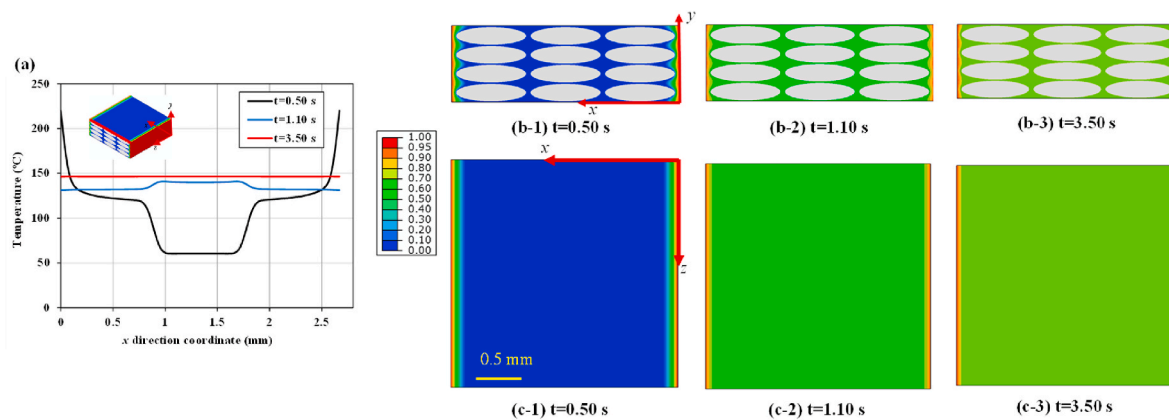


Fig. 7. (a) Temperature profiles along the x direction, (b) and (c) evolution of the degree of cure for UFB specimen in the x-y plane and in the x-z plane.

Table 4 below compares the FP characteristics for cross-ply specimens, including CT, CL, and CLR cases. The FP history of the CT case is depicted in Fig. 8. The front propagation pattern in the CT specimen is identical to that in the UT specimen. In CT and UT specimens, the average front velocity (1.58 mm/s) and degree of cure (94%) are almost the same. This indicates that the laminate layup has insignificant effect on the curing front velocity and degree of cure for cases when the triggering is initiated on the top surface.

The effect of triggering directions on the CL case is presented in Figs. 9 and 10(a). Specifically, the front propagation pattern is different from the UL case. Note that the temperature is plotted along two parallel paths along top and bottom edges for CLR cases (see the red highlighted paths in the insets in Fig. 10), due to the different propagation pattern of the curing front between the upper part and the bottom part. As shown in Figs. 9(a-1), the curing front exhibits a sloped pattern as the front near the bottom surface of CL propagates at a faster velocity than regions near the top surface. The reason is related to the larger concentration of DCPD in the bottom part, which allow more volumetric heat to be transferred to neighboring elements, when compared to the middle and upper parts. In the middle part (Figs. 9(a-1)), the curing front collides with carbon fiber tows that are placed perpendicular to the triggering direction. Thus, the front slows down in upper regions of the laminate. This phenomenon is not observed in the UL case (Fig. 4), where the front moves through the specimen uniformly in the in-plane direction.

The average front velocity in CL is about 35% lower than UL. In Figs. 9(a-2), it can be seen, the front propagated to the right upper corner of CL. The temperature history of the CL case shows that the fiber tow temperature in the right upper corner is lower than other parts, even when the front reaches the right side of the specimen. As mentioned before, the curing front exhibits a sloped propagation pattern. This causes the curing front to propagate from the lower to the upper edges (Figs. 9(a-3)). As the front travels back to the left side, the curing front continues to propagate in a pattern identical to that of UL. But the temperature field is not distributed uniformly, in contrast to the UL case. During the backward movement of the front, the heat collides with the fiber tows perpendicular to the front direction, which results in a temperature decrease. This phenomenon is observed in the UL case. Specifically, by comparing Figs. 4(b-3) to Figs. 9(a-4), the temperature in

**Table 4**  
Comparison of frontal polymerization (FP) process characteristics of cross-ply laminates with different triggering directions.

Specimen	Initial curing duration (s)	Average front velocity (mm/s)	Average degree of cure (%)
CT	0.54	1.58	94.00
CL	0.56	4.59	87.80
CLR	0.17	7.27	99.40

the left side of CL decreases to 180 °C (Fig. 10(a) at t = 3.50 s) while the temperature field in UL is 200 °C (Fig. 4(a) at t = 3.50 s). This higher temperature field in UL leads to a greater value of the degree of cure (95.30%) in comparison with the CL specimen (87.80%), where it shows the backward movement of the curing front.

In Fig. 9(b), the propagation pattern in CLR is similar to that in CL. The front is initiated from the left bottom part of the specimen (Figs. 9(b-1)) and propagate towards the middle region near the top surface. From Figs. 9(b-1)-(b-3), it can be seen that the two fronts do not interact with each other. This causes the middle parts to remain intact with a degree of cure lower than 10%. Specifically at 0.10 s and 0.20 s, the temperature graphs show the temperature are 60~80 °C in regions near the top surface (see Figs. 10(b-1)). Furthermore, the front in both CL and CLR cases forms a sloped shape (see Fig. 11(a)). This phenomenon is more noticeable in the CLR specimen. The middle near the top surface experiences low temperatures (Figs. 10(b-1) at t = 0.10 s). As the two fronts propagate through the middle region of the laminate, the slope of the front, that is linearly fitted, decreases from 2.14 to 1.52. This slope clearly indicates the impact of composite layup on the propagation pattern.

In Figs. 10(b-2), at t = 0.20 s, the thermal spike forms near the bottom part and the temperature rapidly rises to 256 °C for the CLR case. Fig. 11(b) shows how the fiber direction significantly affects the thermal behaviors of the composite laminates. Specifically, the unidirectional case has a temperature of 355 °C at thermal spike moment, which is about 100 °C higher than that of the cross-ply case. Additionally, the thermal spike in woven CFRP experimentally reported by Centellas et al. [46] is 157 °C. Based on the result in Fig. 11(b), the difference between the experimental results and our predicted values should come from the different carbon fiber architectures (i.e., woven, unidirectional vs. cross-ply), which merits further investigation. Moreover, the fiber volume fraction also plays a significant role in the maximum temperature. In the experiments of Centellas et al. [55], the fiber volume fraction of their woven composites is 47~52%, whereas in our simulation, the fiber volume fraction is 36%. In our prior modeling work [17], we have found that the maximum temperature dropped by about 15% when the fiber volume fraction increased from 0 to 67%. Therefore, the difference in the temperature thermal spikes is jointly impacted by the differences in the carbon fiber architecture and the fiber volume fraction.

Fig. 12 compares the front location vs. time for the unidirectional and cross-ply cases. Specifically, the multiple-front cases (see Fig. 12(a)), including ULR and CLR cases, show a continuous and an approximate linear front velocity in the polymerization process. In comparison, the front velocity changes within different range of time for single-front cases, including the UL and CL cases. The cross-ply layup reduced the lower front velocity when comparing the CL case to the UL case. These findings are also prominent in UT and CT cases (see Fig. 12(b)), where the front velocity is not steady in single front cases. Additionally, the

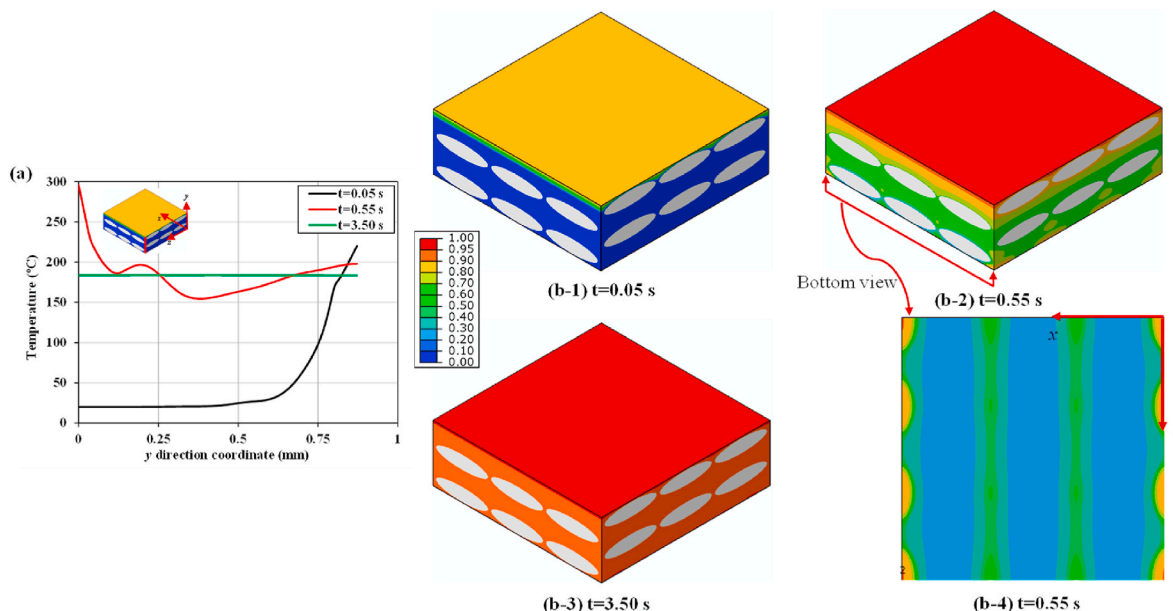


Fig. 8. (a) Temperature profiles along the y direction, (b) and (c) evolution of the degree of cure field for CT specimen.

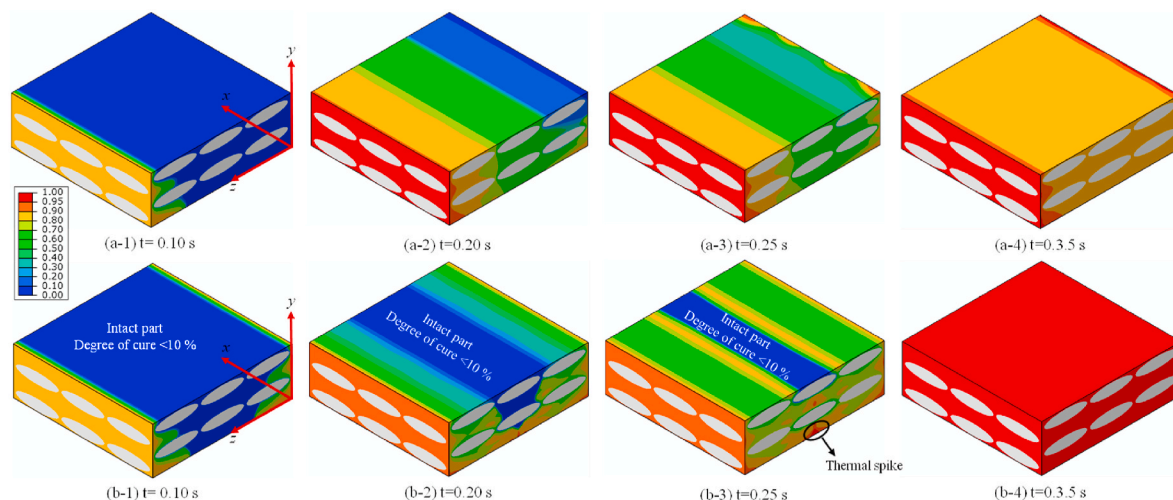


Fig. 9. Evolution of the degree of cure field for (a) CL and (b) CLR specimens.

cross-ply laminate CT case exhibits a lower front velocity in different times than the UT case.

Generally, comparing the FP characteristics of unidirectional and cross-ply laminates showed that single-triggering direction parallel to the fiber direction results into faster polymerization and higher degree of cure. For unidirectional laminates, the ULR triggering method is preferred and recommended due to the higher front velocity (48%) and higher degree of cure (4%), when compared to the UL triggering case. For the cross-ply laminates, the CLR triggering method is preferred and recommended, because the CLR triggering case shows 86% higher in the front velocity and 11.60% higher in the degree of cure, when compared to the CL case.

#### 4.2. Effect of thermal conductivity

To investigate the thermal conductivity of the fiber on the FP performance, additional simulations were performed using laminates with glass and Kevlar fibers. Note that the difference in the FP performance is due to the different thermophysical properties of the fibers (see Table 2),

in which the thermal conductivity plays the most critical role. Fig. 13 shows the predicted curing front location vs. time for the ULR and CLR cases of laminates with carbon, glass, and Kevlar fibers. It is shown that the front velocity drastically decreases as the thermal conductivity decreases from 10.45 W/m·K (for carbon fiber) to 1.14 W/m·K (for glass fiber) and 0.04 W/m·K (for Kevlar fiber). Specifically, for ULR cases, the average front velocity is only 0.07 mm/s for the Kevlar fiber laminate and 0.76 mm/s for the glass fiber laminate, in contrast to 9.13 mm/s for the carbon fiber laminate. Additionally, for ULR cases, the front position in carbon and glass fiber laminates follows a linear trend in comparison with that of the Kevlar fiber laminate, in which it plateaus at around  $t = 1.00$  s. Moreover, decreasing the thermal conductivity also significantly reduces the degree of cure. Specifically, for the glass fiber laminate, where the thermal conductivity is 90% lower than the carbon fiber, the average degree of cure is only 79%, which is 20% lower than that of the carbon fiber laminate. For the Kevlar fiber laminate, due to having the lowest thermal conductivity, the curing front distinguishes during the propagation after 1 s and the average degree of cure only reached 22%.

A similar trend is observed for CLR cases when compared to ULR

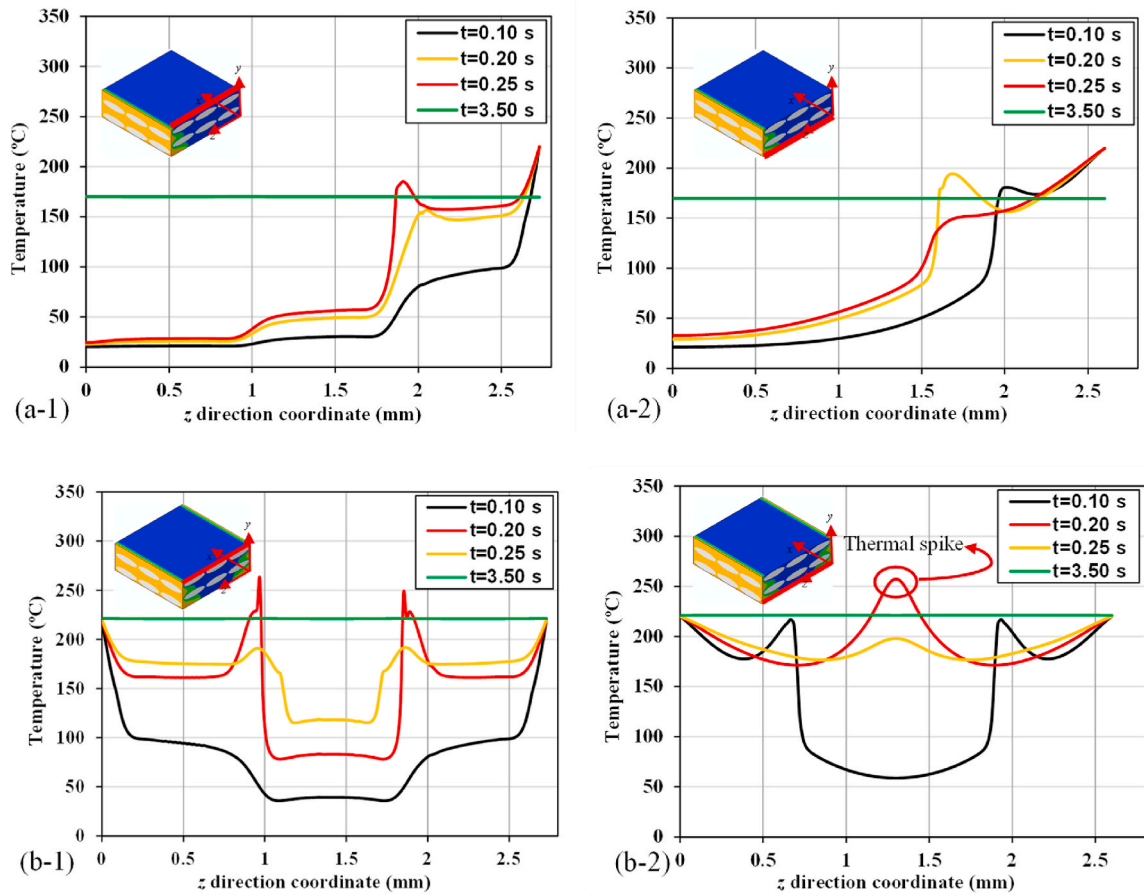


Fig. 10. Temperature profiles along z direction for (a) CL and (b) CLR specimens at varying times.

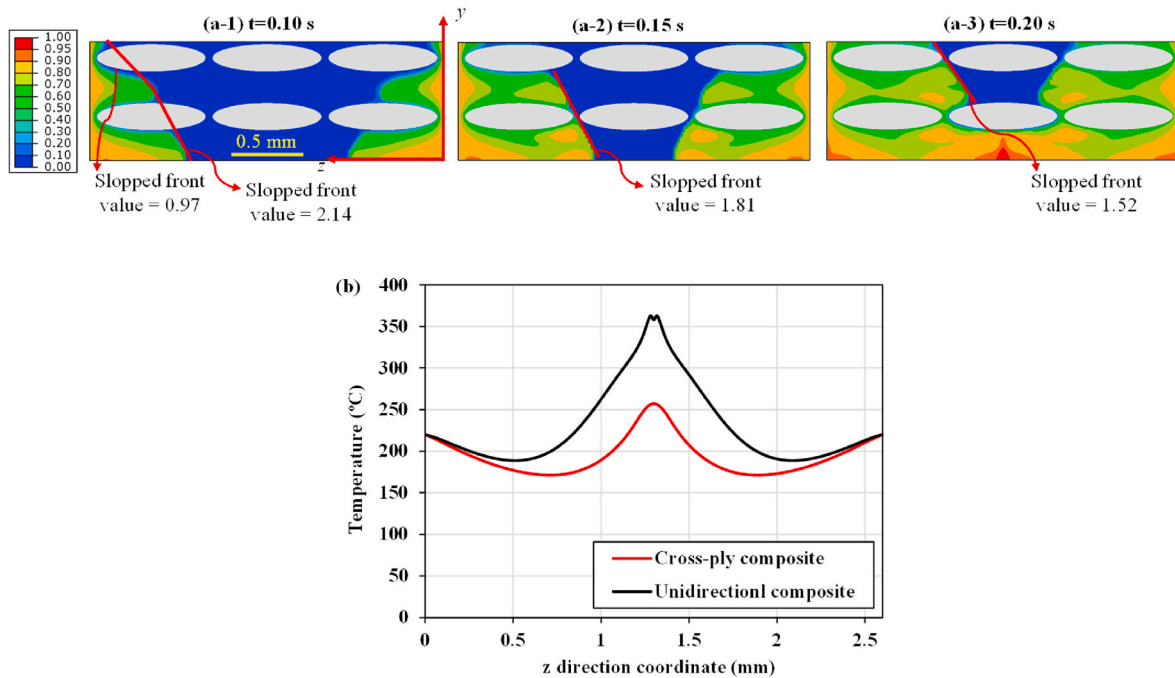


Fig. 11. Sloped pattern of the curing front in CLR laminate (front view).

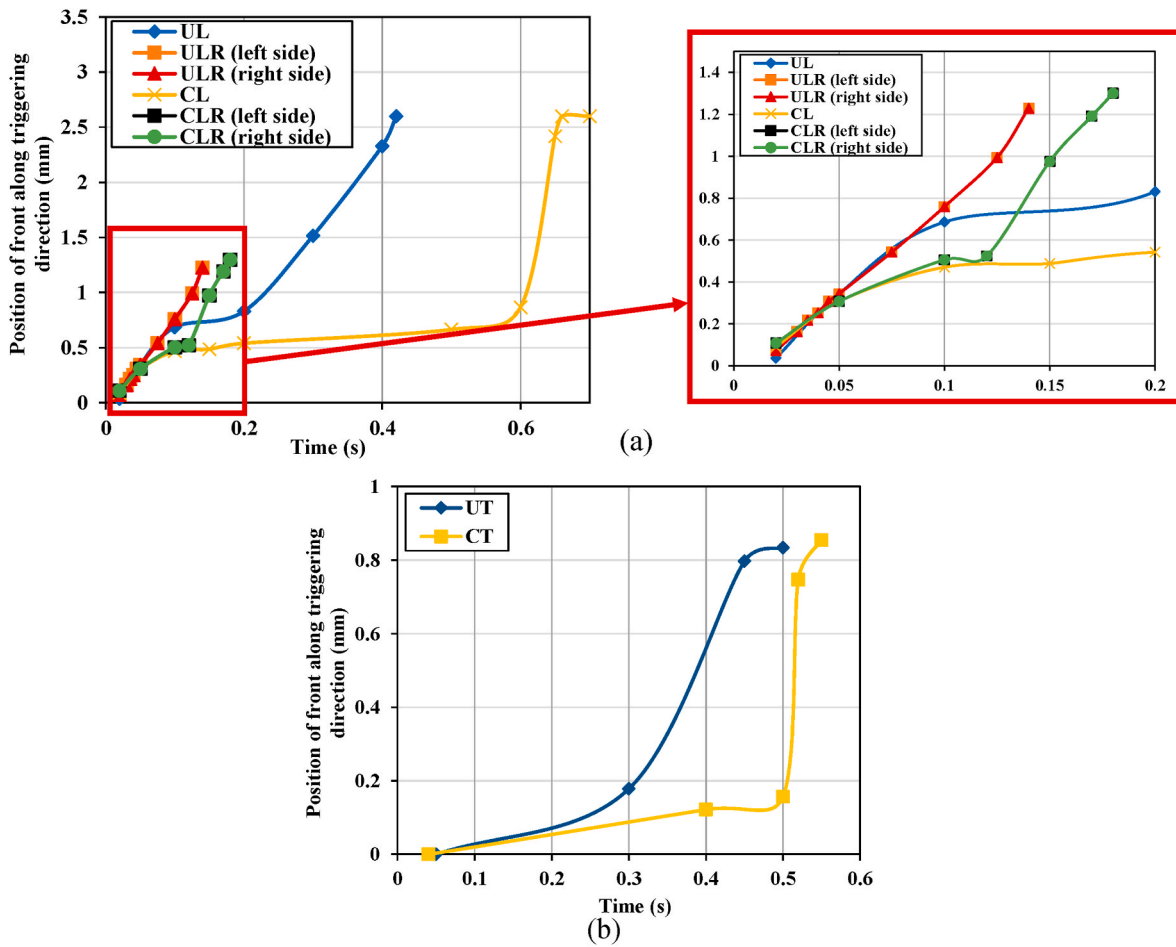


Fig. 12. Curing front location vs. time for (a) side triggering and (b) top triggering cases.

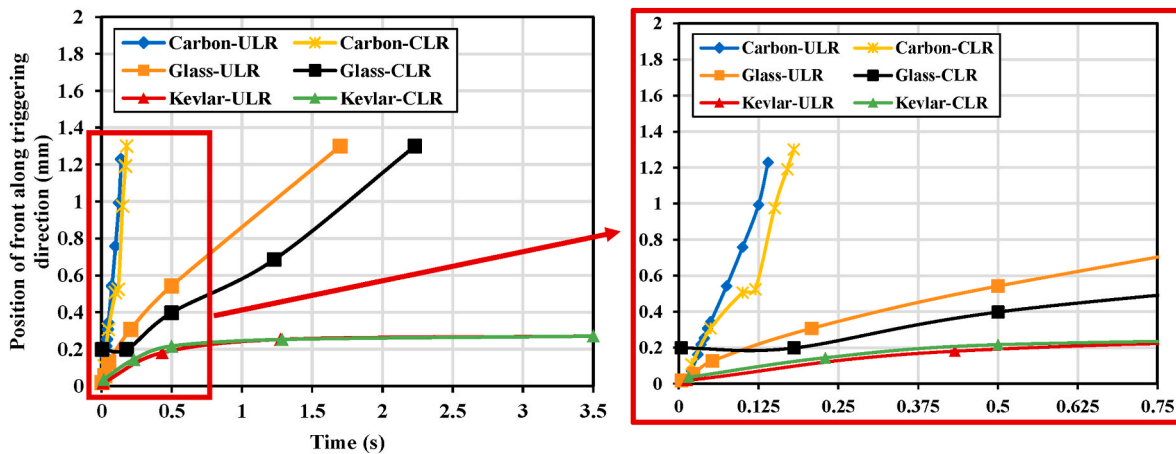


Fig. 13. Curing front location vs. time in the composite laminates with carbon, glass, and Kevlar fibers for the ULR and CLR cases.

cases with different fibers, as shown in Fig. 13. Generally, changing the layup from unidirectional to cross-ply increases the overall curing duration, and thus, decreases the front velocity. The reduction in the front velocity is more pronounced in the CLR case with glass fiber, where the average front velocity is only 0.58 mm/s, which is 13% lower than its ULR case. The average degree of cure for the glass fiber CLR case is 68%, which is 14% lower than its ULR case. For the Kevlar fiber laminate, the average front velocity and degree of cure for the CLR case are identical to its ULR case.

Fig. 14 (a) compares the sloped pattern formed across the thickness direction during the front propagation for CLR cases of Kevlar and glass fiber laminates. Specifically, the front in the Kevlar fiber laminate moves uniformly along the propagating direction, and thus, the sloped pattern is not formed. This phenomenon is due to the low thermal conductivity of Kevlar fiber, which indicates a minimum heat exchange between the fiber and the resin, and hence, the resin is the only medium for the heat conduction. Therefore, due to the low thermal conductivity of the resin, the front propagates slowly and finally distinguishes at around  $t = 1.00$

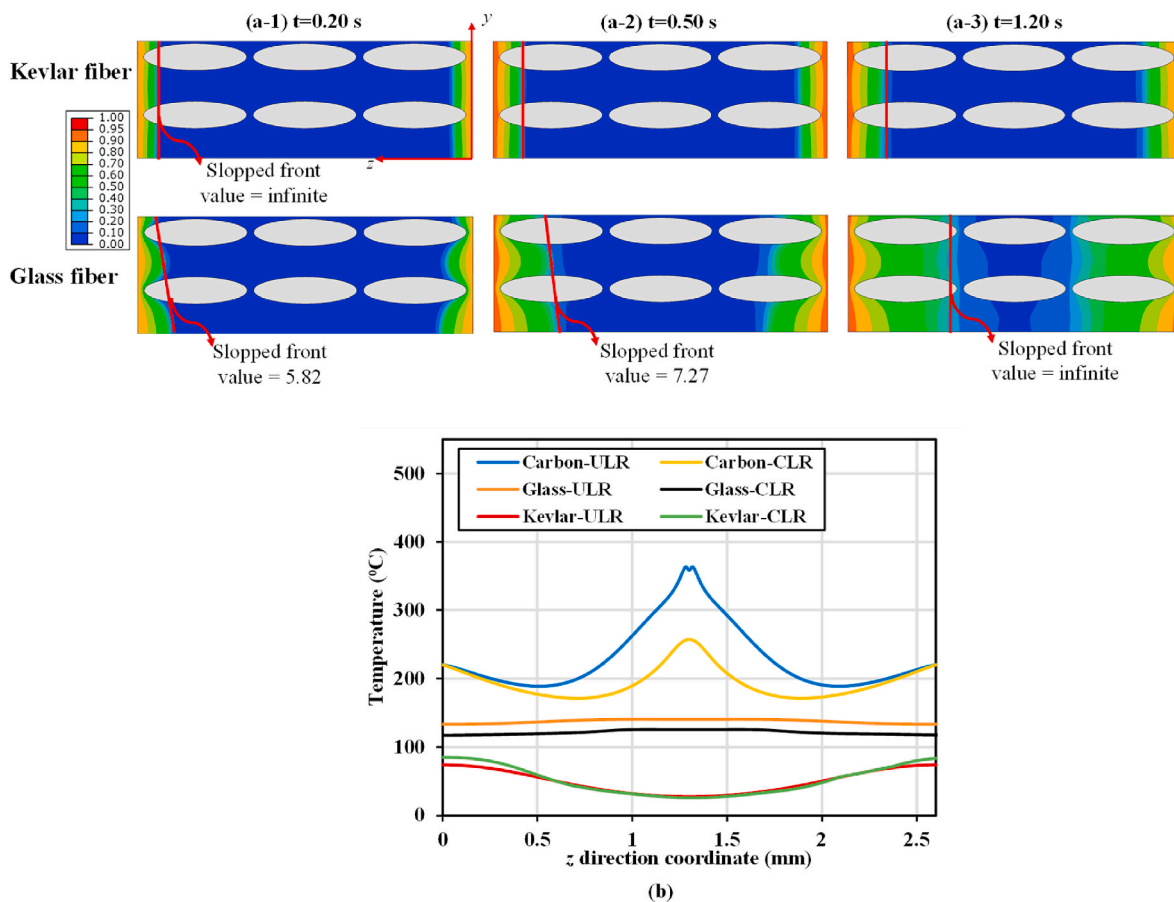


Fig. 14. (a) Comparison of sloped pattern of the curing front in the glass and Kevlar fiber composite laminates for the CLR case (front view) and (b) comparison of the temperature profiles along the  $z$  direction of composites with carbon, glass, and Kevlar fibers for the ULR and CLR cases.

s. As such, the thermal spike also disappears (see Fig. 14 (b)). For the CLR case with glass fiber laminate, since the thermal conductivity is higher than Kevlar fiber, the sloped pattern still forms during the propagation at  $t = 0.20$  s. After that, the front gradually returns to a vertical position, as shown in Fig. 14. Overall, it is shown that the higher the thermal conductivity, the lower the slope of the front. Additionally, the front temperature at the thermal spike moment significantly drops as the thermal conductivity reduces. As shown in Fig. 14(b), the thermal spike temperature dropped from 255 °C and 355 °C for the carbon fiber CLR and ULR cases to only 133 °C and 117 °C for the glass fiber ULR and CLR cases. For cases with the Kevlar fiber, the thermal spike is not formed.

## 5. Conclusions

In this study, 3D frontal modeling in unidirectional and cross-ply carbon fiber reinforced DCPD matrix composites was conducted to investigate the effects of laminate layup, triggering direction, and the thermal conductivity of the fiber on the frontal polymerization (FP) process, including the degree of cure, curing front velocity, and temperature distributions. The 3D frontal modeling was achieved using finite element analysis with ABAQUS, accompanied by two coupled user subroutines, *i.e.*, the heat flux subroutine (HETVAL) and the user defined field subroutine (USDFLD), that are developed to implement the heat transfer and cure kinetics equation in a 3D computational domain. The subroutines are validated with 1D and 2D modeling and experimental data. The findings lead mainly to the following conclusions:

- Triggering from both the left and right sides (*i.e.*, ULR and CLR cases) results in a higher front velocity and can allow the composites to

achieve a higher average degree of cure, when compared to cases where triggering is initiated from only one side (*i.e.*, UL, UT, CL, and CT cases). For example, the average front velocity of the CLR case is 86% higher than the CL case and 360% higher than the CT case. The average degree of cure of the CLR case is 11.60% higher than the CL case and 5.40% higher than the CT case. Hence, the ULR and CLR cases present better performance in practical applications.

- Triggering in the direction perpendicular to the fiber direction is not preferred. It was found that degree of cure in the UF and UFB specimens is, on average, 20% and 70%, respectively, lower than those in the ULR, UL, and UT cases.
- The laminate layup (*i.e.*, unidirectional vs. cross-ply) essentially influences the relative positions between the fiber tows and the triggering direction. The average front velocity in CT, CL, and CLR cases decreases by 20~25% in comparison to UT, UL, and ULR cases. Moreover, the front propagates in a sloped pattern in cross-ply laminates, as opposed to the traditionally observed uniform pattern in unidirectional laminates.
- The front velocity and the degree of cure are expected to be greatly reduced in laminates with fibers that have lower thermal conductivity when compared to the carbon fiber laminates, such as in glass fiber (92% reduction in front velocity and 20% reduction in average degree of cure for the ULR case) and Kevlar fiber (99% reduction in front velocity and 78% reduction in average degree of cure for the ULR case) laminates.
- The laminate layup also significantly affects the maximum temperature of the thermal spike for cases with both left and right triggering front. Specifically, it was found that the thermal spike temperature in a CLR carbon fiber laminate is about 100 °C lower than its ULR case. Moreover, laminates using fibers with a lower thermal conductivity

are expected to show reduced temperature at the thermal spike and could even lead to not forming the thermal spike (e.g., Kevlar fiber).

The aforementioned findings are envisaged to provide guidance in the control and optimization of the FP process for manufacturing CFRP composites. Other parameters, including the weight fractions of the initiators and the uniformity of the dispersion of the initiators in the monomer, could also impact the FP process in addition to those factors examined in this study. These variables can affect the monomer mixture's thermal characteristics and cure kinetics, which would change the behavior of the FP. These factors may also influence the viscosity of the resin mixture, which changes capillary flow through the fiber tow's microstructure and, consequently, alters the intra-tow FP process. Due to the capillary effect and the permeability of the fiber tow, these factors, alongside with the fiber microstructures and composite layout, are anticipated to jointly affect the intra-tow FP process, which need to be further studied.

#### CRedit authorship contribution statement

Amirreza Tarafdar: Investigation, Methodology, Formal analysis, Writing - Original Draft, Data curation. Chen Jia: Investigation, Formal analysis, Data curation. Weifei Hu: Writing - review & editing. Ian Hosein: Supervision, Writing - review & editing, Funding acquisition. Kun (Kelvin) Fu: Writing - review & editing. Yeqing Wang: Conceptualization, Methodology, Supervision, Formal analysis, Writing - review & editing, Funding acquisition.

#### Declaration of competing interest

The authors declare that they have no known competing financial interests or personal relationships that could have appeared to influence the work reported in this paper.

#### Data availability

Data will be made available on request.

#### Acknowledgments

A. Tarafdar, Y. Wang, and I. Hosein would like to acknowledge the financial support from National Science Foundation under Award No. CMMI-2208130.

#### Appendix A. Supplementary data

Supplementary data to this article can be found online at <https://doi.org/10.1016/j.compositesb.2023.111029>.

#### References

- Zhang G, Song D, Jiang J, Li W, Huang H, Yu Z, et al. Electrically assisted continuous vat photopolymerization 3D printing for fabricating high-performance ordered graphene/polymer composites. *Compos B Eng* 2023;250:110449.
- Tarafdar A, Razmkhah O, Ahmadi H, Liaghat G, Chitsaz Charandabi S, Rezaei Faraz M. Effect of layering layout on the energy absorbance of bamboo-inspired tubular composites. *J Reinforc Plast Compos* 2022;41(15–16):602–23.
- Liu X, Zhou J, Zhao J, Liu S. Design and synthesis of polyetherimides as a flame-retarded thermolatent hardener for high-performance epoxy thermosets. *Compos B Eng* 2023;259:110754.
- Faraz MR, Ahmadi H, Liaghat G, Vahid S, Razmkhah O, Tarafdar A. Energy absorption assessment of bio-mimicked hybrid Al/PP sandwich tube: experimental and Numerical Investigation. *Thin-Walled Struct* 2022;181:110116.
- De Noni L, Zorzetto L, Briatico-Vangosa F, Rink M, Ruffoni D, Andena L. Modelling the interphase of 3D printed photo-cured polymers. *Compos B Eng* 2022;234:109737.
- Choi EY, Kim CK, Park CB. Fabrication of MA-EPDM grafted MWCNTs by reactive extrusion for enhanced interfacial adhesion and mechanical properties of PP/MA-EPDM composite. *Compos B Eng* 2022;242:110043.
- Uitz O, Koirala P, Tehrani M, Seepersad CC. Fast, low-energy additive manufacturing of isotropic parts via reactive extrusion. *Addit Manuf* 2021;41:101919.
- Odom MGB, Sweeney CB, Parviz D, Sill LP, Saed MA, Green MJ. Rapid curing and additive manufacturing of thermoset systems using scanning microwave heating of carbon nanotube/epoxy composites. *Carbon* 2017;120:447–53.
- Sangermano M, D'Anna A, Marro C, Klikovits N, Liska R. UV-activated frontal polymerization of glass fibre reinforced epoxy composites. *Compos B Eng* 2018;143:168–71.
- Deng K, Zhang C, Fu K. Additive manufacturing of continuously reinforced thermally curable thermoset composites with rapid interlayer curing. *Compos B Eng* 2023;257:110671.
- Knaack P, Klikovits N, Tran AD, Bomze D, Liska R. Radical induced cationic frontal polymerization in thin layers. *J Polym Sci Polym Chem* 2019;57(11):1155–9.
- Scazzosi R, Bregão de Souza SD, Amico SC, Giglio M, Manes A. Experimental and numerical evaluation of the perforation resistance of multi-layered alumina/aramid fiber ballistic shield impacted by an armor piercing projectile. *Compos B Eng* 2022;230:109488.
- Adhikari D, Gururaja S, Hemchandra S. Resin infusion in porous preform in the presence of HPM during VARTM: flow simulation using level set and experimental validation. *Compos Appl Sci Manuf* 2021;151:106641.
- Walczyk D, Koppers J. Thermal press curing of advanced thermoset composite laminate parts. *Compos Appl Sci Manuf* 2012;43(4):635–46.
- Tarafdar A, Liaghat G, Ahmadi H, Razmkhah O, Chitsaz Charandabi S, Rezaei Faraz M, et al. Quasi-static and low-velocity impact behavior of the bio-inspired hybrid Al/GFRP sandwich tube with hierarchical core: experimental and numerical investigation. *Compos Struct* 2021;276:114567.
- Robertson ID, Yourdkhani M, Centellas PJ, Aw JE, Ivanoff DG, Goli E, et al. Rapid energy-efficient manufacturing of polymers and composites via frontal polymerization. *Nature* 2018;557(7704):223–7.
- Goli E, Peterson SR, Geubelle PH. Instabilities driven by frontal polymerization in thermosetting polymers and composites. *Compos B Eng* 2020;199:108306.
- Goli E, Parikh NA, Yourdkhani M, Hibbard NG, Moore JS, Sottos NR, et al. Frontal polymerization of unidirectional carbon-fiber-reinforced composites. *Compos Appl Sci Manuf* 2020;130:105689.
- Chekanov YA, Pojman JA. Preparation of functionally gradient materials via frontal polymerization. *J Appl Polym Sci* 2000;78(13):2398–404.
- Nuvoli D, Alzari V, Pojman JA, Sanna V, Ruiu A, Sanna D, et al. Synthesis and characterization of functionally gradient materials obtained by frontal polymerization. *ACS Appl Mater Interfaces* 2015;7(6):3600–6.
- Chen S, Sui J, Chen L, Pojman JA. Polyurethane–nanosilica hybrid nanocomposites synthesized by frontal polymerization. *J Polym Sci Polym Chem* 2005;43(8):1670–80.
- Yan Q-Z, Zhang W-F, Lu G-D, Su X-T, Ge C-C. Frontal polymerization synthesis of starch-grafted hydrogels: effect of temperature and tube size on propagating front and properties of hydrogels. *Chem Eur J* 2006;12(12):3303–9.
- Guo X, Wang C-F, Fang Y, Chen L, Chen S. Fast synthesis of versatile nanocrystal-embedded hydrogels toward the sensing of heavy metal ions and organoamines. *J Mater Chem* 2011;21(4):1124–9.
- Sanna R, Alzari V, Nuvoli D, Scognamiglio S, Marceddu S, Mariani A. Polymer hydrogels of 2-hydroxyethyl acrylate and acrylic acid obtained by frontal polymerization. *J Polym Sci Polym Chem* 2012;50(8):1515–20.
- Nagy IP, Sike L, Pojman JA. Thermochromic composite prepared via a propagating polymerization front. *J Am Chem Soc* 1995;117(12):3611–2.
- White SR, Kim C. A simultaneous lay-up and in situ cure process for thick composites. *J Reinforc Plast Compos* 1993;12(5):520–35.
- Kim C, Teng H, Tucker CL, White SR. The continuous curing process for thermoset polymer composites. Part 1: modeling and demonstration. *J Compos Mater* 1995;29(9):1222–53.
- Wang Y, Lampkin S. Rapid curing of epoxy resin using self-sustained frontal polymerization towards the additive manufacturing of thermoset fiber composites. In: 37th annual American society for composites technical conference; 2022. p. 19–21. Tucson, Arizona, September.
- Vallons KAM, Drozdak R, Charret M, Lomov SV, Verpoest I. Assessment of the mechanical behaviour of glass fibre composites with a tough polydicyclopentadiene (PDCPD) matrix. *Compos Appl Sci Manuf* 2015;78:191–200.
- Datta P, Efimenko K, Genzer J. The effect of confinement on thermal frontal polymerization. *Polym Chem* 2012;3(12):3243–6.
- Robertson ID, Pruitt EL, Moore JS. Frontal ring-opening metathesis polymerization of exo-dicyclopentadiene for low catalyst loadings. *ACS Macro Lett* 2016;5(5):593–6.
- Alzari V, Nuvoli D, Sanna D, Ruiu A, Mariani A. Effect of limonene on the frontal ring opening metathesis polymerization of dicyclopentadiene. *J Polym Sci Polym Chem* 2016;54(1):63–8.
- Mariani A, Fiori S, Chekanov Y, Pojman JA. Frontal ring-opening metathesis polymerization of dicyclopentadiene. *Macromolecules* 2001;34(19):6539–41.
- Ruiu A, Sanna D, Alzari V, Nuvoli D, Mariani A. Advances in the frontal ring opening metathesis polymerization of dicyclopentadiene. *J Polym Sci Polym Chem* 2014;52(19):2776–80.
- Goli E, Robertson ID, Geubelle PH, Moore JS. Frontal polymerization of dicyclopentadiene: a numerical study. *J Phys Chem B* 2018;122(16):4583–91.
- Tran AD, Koch T, Liska R, Knaack P. Radical-induced cationic frontal polymerisation for prepreg technology. *Monatshefte für Chemie - Chemical Monthly* 2021;152(1):151–65.

- [37] Solovyov SE, Ilyashenko VM, Pojman JA. Numerical modeling of self-propagating polymerization fronts: the role of kinetics on front stability. *Chaos: Interdiscipl J Nonlinear Sci* 1997;7(2):331–40.
- [38] Goldfeder PM, Volpert VA, Ilyashenko VM, Khan AM, Pojman JA, Solovyov SE. Mathematical modeling of free-radical polymerization fronts. *J Phys Chem B* 1997;101(18):3474–82.
- [39] Liu H, Wei H, Moore JS. Frontal ring-opening metathesis copolymerization: deviation of front velocity from mixing rules. *ACS Macro Lett* 2019;8(7):846–51.
- [40] Goli E, Robertson ID, Agarwal H, Pruitt EL, Grolman JM, Geubelle PH, et al. Frontal polymerization accelerated by continuous conductive elements. *J Appl Polym Sci* 2019;136(17):47418.
- [41] Vyas S, Goli E, Zhang X, Geubelle PH. Manufacturing of unidirectional glass-fiber-reinforced composites via frontal polymerization: a numerical study. *Compos Sci Technol* 2019;184:107832.
- [42] Gao Y, Li S, Kim J-Y, Hoffman I, Vyas SK, Pojman JA, et al. Anisotropic frontal polymerization in a model resin–copper composite. *Chaos: Interdiscipl J Nonlinear Sci* 2022;32(1):013109.
- [43] Topkaya T, Gao Y, Geubelle PH. Frontal polymerization in short-fiber-reinforced thermoset composites. *ACS Appl Polym Mater* 2022;4(10):6880–6.
- [44] Wang Y. Modeling the through-thickness frontal polymerization of unidirectional carbon fiber thermoset composites: effect of microstructures. *J Appl Polym Sci* 2022;139(31):e52735.
- [45] Frulloni E, Salinas MM, Torre L, Mariani A, Kenny JM. Numerical modeling and experimental study of the frontal polymerization of the diglycidyl ether of bisphenol A/diethylenetriamine epoxy system. *J Appl Polym Sci* 2005;96(5):1756–66.
- [46] Centellas PJ, Yourdkhani M, Vyas S, Koohbor B, Geubelle PH, Sottos NR. Rapid multiple-front polymerization of fiber-reinforced polymer composites. *Compos Appl Sci Manuf* 2022;158:106931.
- [47] Hexcel. **HexTow® AS4 carbon fiber datasheet**.
- [48] Potter E, Pinho ST, Robinson P, Iannucci L, McMillan AJ. Mesh generation and geometrical modelling of 3D woven composites with variable tow cross-sections. *Comput Mater Sci* 2012;51(1):103–11.
- [49] Sherburn M. Geometric and mechanical modelling of textiles. University of Nottingham United Kingdom; 2007.
- [50] Barwick SC, Papanthasiou TD. Identification of fiber misalignment in continuous fiber composites. *Polym Compos* 2003;24(3):475–86.
- [51] Morita S, Ueda M, Takahashi T, Kajiwara K, Yoshimura A, Sugiura N. Performance assessment for fiber tracking of unidirectional carbon fiber reinforced plastic by digital image correlation of X-ray computed-tomography. *Adv Compos Mater* 2022:1–13.
- [52] [www.matweb.com. Kevlar-aramid fiber. https://www.matweb.com/search/datasheet.aspx?matguid=77b5205f0dcc43bb8cbe6fee7d36cbb5](https://www.matweb.com/search/datasheet.aspx?matguid=77b5205f0dcc43bb8cbe6fee7d36cbb5).
- [53] Struzziero G, Teuwen JJE. Effect of convection coefficient and thickness on optimal cure cycles for the manufacturing of wind turbine components using VARTM. *Compos Appl Sci Manuf* 2019;123:25–36.